Heliyon 10 (2024) e35461

Contents lists available at ScienceDirect

Heliyon

journal homepage: www.cell.com/heliyon

Research article

TMAO is involved in kidney-yang deficiency syndrome diarrhea by mediating the "gut-kidney axis"

Shiqin Xie [a,b], Na Deng [a,b], Leyao Fang [a,b], Junxi Shen [a,b], Zhoujin Tan [a,b,*], Ying Cai [a,b,**]

[a] College of Traditional Chinese Medicine, Hunan University of Chinese Medicine, Changsha, Hunan, China
[b] Hunan Key Laboratory of Traditional Chinese Medicine Prescription and Syndromes Translational Medicine, Changsha, Hunan, China

ARTICLE INFO

Keywords:
Gut-kidney axis
TMAO
Kidney-yang deficiency syndrome diarrhea
Intestinal microbiota
Inflammation
Renal fibrosis
Intestinal barrier

ABSTRACT

Background: Trimethylamine-N-oxide (TMAO) is a harmful metabolite dependent on the intestinal microbiota and excreted through the kidneys. According to numerous investigations, rich circulation concentrations of TMAO have been linked to kidney and gastrointestinal disorders. Through the "gut-kidney axis" mediated by TMAO, this research attempted to clarify the microbiological causes of kidney-yang deficiency syndrome diarrhea.

Methods: Adenine and *Folium Sennae* were used to create a mouse model of kidney-yang deficiency syndrome diarrhea. 16S rRNA sequencing was used to identify the traits of the intestinal mucosal microbiota. ELISA was used to assess TMAO, transforming growth factor-β1 (TGF-β1), interleukin-1β (IL-1β), and NOD-like receptor thermal protein domain associated protein 3 (NLRP3). Kidney tissue fibrosis was evaluated using Masson's trichrome staining, and immunohistochemical labeling was used to investigate the protein expression of occludin and Zonula Occludens-1 (ZO-1) in small intestine tissue. Microbial activity was determined by using fluorescein diacetate (FDA) hydrolysis spectrophotometry.

Results: TMAO showed a positive correlation with NLRP3, IL-1β and TGF-β1, all of which exhibited substantial increases ($P < 0.05$). Significant renal fibrosis and decreased ZO-1 and occludin expression in small intestine tissues were detected in the model group. The sequencing results revealed alterations in both α and β diversities of small intestinal mucosal microbiota. Elevated TMAO concentrations were potentially associated with increasing Firmicutes/Bacteroidota (F/B) ratios, *Streptococcus*, *Pseudomonas* and *unclassified Clostridia* UCG 014, but with decreasing *Rothia* and *RB41 abundances*.

Conclusion: This study establishes a link between intestinal microbiota dysbiosis and elevated TMAO concentrations. TMAO can activate inflammatory responses and cytokines, contributing to kidney-yang deficiency syndrome diarrhea via the "gut-kidney axis". Moreover, TMAO may coincide with disruptions in the intestinal barrier and renal fibrosis. Dysfunction of the "gut-kidney axis" further elevates TMAO levels, perpetuating a vicious cycle.

* Corresponding author. College of Traditional Chinese Medicine, Hunan University of Chinese Medicine, Changsha, Hunan, China.
** Corresponding author. College of Traditional Chinese Medicine, Hunan University of Chinese Medicine, Changsha, Hunan, China.
E-mail addresses: tanzhjin@sohu.com (Z. Tan), 31650124@qq.com (Y. Cai).

https://doi.org/10.1016/j.heliyon.2024.e35461
Received 17 March 2024; Received in revised form 28 July 2024; Accepted 29 July 2024
Available online 30 July 2024

1. Introduction

When red meat, seafood, shellfish, dairy products and so on are consumed, dietary components such as carnitine, choline and betaine are metabolized by gut bacteria to generate trimethylamine (TMA). TMA travels to the liver via the portal vein after being taken up by intestinal epithelial cells for absorption. In the liver, TMAO is produced through the oxidation of TMA by hepatic flavin monooxygenase (FMO). Ultimately, TMAO is eliminated from the body primarily by the kidneys [1–3]. Diet, the composition of the intestinal microbiota, and the activity of hepatic FMO all influence the levels of TMAO [4]. Imbalances in choline metabolism can lead to increased production of TMA by intestinal microbiota, thereby raising TMAO levels [5]. Although TMAO can stabilize protein folding, extensive research supports its role as a harmful substance implicated in the development of diseases [6–8]. The relative risk of all-cause mortality increases by 7.6 % for every 10 μmol/L increase in TMAO, as indicated by a dose-response meta-analysis [9]. Berberine (BBR) and resveratrol (RSV) can reshape the intestinal microbiota, which can help prevent the formation of TMA and subsequently lower TMAO levels [10,11].

The "gut-kidney axis," which is defined by a bidirectional pathogenic relationship between kidney disease and intestinal microbiota, is the primary area of involvement for TMAO [12]. On the one hand, TMAO, a nitrogen-containing molecule, is thought to be a uremic toxin that is produced when the gut bacteria breaks down substrates like choline [13]. It causes increasing renal fibrosis and dysfunction and accelerates the development of chronic kidney disease (CKD) [8,14]. On the other hand, TMAO influences the intestinal microbiota's composition and metabolism, which results in dysbiosis and disruption of the intestinal barrier [15]. This ultimately increases the host's exposure to endotoxins and exacerbates renal damage and creates a vicious cycle.

TMAO can induce inflammatory responses [16]. The transmission of inflammatory cytokines through the "gut-kidney axis" is involved in diarrhea [17,18]. Small intestinal mucosal microbiota alterations are closely related to diarrhea [19–21]. The small intestine is a secretory and absorptive organ, and by controlling intestinal motility, absorption and secretion, its receptors play a role in diarrhea [22]. In traditional Chinese medicine, kidney-yang deficiency syndrome diarrhea is characterized by abdominal rumbling, umbilical pain relief after defecation, thin and unformed stools mixed with undigested food [23], similar to small intestinal diarrhea.

Our previous research demonstrated that kidney-yang deficiency syndrome diarrhea results in inflammatory responses [17,24]. Therefore, we hypothesize that dysbiosis of intestinal microbiota is associated with variations in TMAO concentrations. TMAO contributes to kidney-yang deficiency syndrome diarrhea by regulating inflammatory cytokine transmission through "gut-kidney axis". This study focused on the intestinal microbiota to determine the correlation between TMAO concentration and the inflammatory response, renal fibrosis and intestinal barrier damage.

2. Materials and methods

2.1. Materials

2.1.1. Animals

Sex hormones can influence the dimorphism of the intestinal microbiota to some degree [25], male mice were initially chosen for this study. Hunan Slake Jinda Experimental Animal Co., Ltd. (China, Animal Quality Certificate No. 430727231101380948) provided fourteen four-week-old, specific pathogen-free (SPF) Kunming mice. All mice were kept in regulated settings at the Hunan University of Chinese Medicine's Animal Experiment Centre. Hunan Slake Jinda Experimental Animal Co., Ltd. supplied the feed (license number. SYXK (Xiang) 2019-0004). The Animal Care and Use Committee of Hunan University of Chinese Medicine approved the guidelines that were adhered to in all animal research (Approval No. LL2023081010).

2.1.2. Drugs

Adenine suspension (Changsha Yael Biotechnology Co., Ltd., EZ27890C450): Adenine was prepared at 50 mg/kg in sterile water [26].

Folium Sennae decoction (The First Affiliated Hospital of Hunan University of Traditional Chinese Medicine, 2008232): 1 g/mL was the concentration of a decoction made from raw herbs.

2.1.3. Reagents

FDA stock solution: 1 mL of acetone was combined with 2 mg of FDA.

FDA reaction mixture: PBS was mixed with the FDA reserve solution at a concentration of 10 μg/mL.

Occludin rabbit pAb antibody (Servicebio, Wuhan, Hubei, GB111401) was used at a 1:500 dilution.

ZO-1 rabbit pAb antibody (Servicebio, Wuhan, Hubei, GB111402) was used at a 1:500 dilution.

HRP-conjugated goat anti-rabbit secondary antibody (Servicebio, Wuhan, Hubei, GB23303) was used at a 1:200 dilution.

2.1.4. Reagent kits

TMAO ELISA Kit (No. SU-B20977), NLRP3 ELISA Kit (No. CK-E21160), an IL-1β ELISA Kit (No. CK-E20533) and a TGF-β1 ELISA Kit (No. CK-E20217) were purchased from Quanzhou Kenuodi Biotechnology Co., Ltd.

2.2. Methods

2.2.1. Grouping and modeling of animals

A random number table technique was used to assign the mice, following a 3-day adaption period, into two groups: a control group (C, n = 7) and a kidney-yang deficiency syndrome diarrhea group (KYDD, n = 7). After receiving 50 mg/kg adenine suspension (0.4 mL/each) once daily for fourteen days, mice in the KYDD group were also administered 10 g/kg *Folium Sennae* decoction (0.4 mL/each) once daily for seven days beginning on the eighth day. The identical timing and volume of sterile water were administered to the C group [27].

2.2.2. Model evaluation criteria

The diagnostic criteria outlined in the "Consensus Opinion on TCM Diagnosis and Treatment of Diarrhea (2017) " were used as the basis for evaluating indicators of kidney-yang deficiency syndrome diarrhea in the model [28]. The diagnostic criteria included increased loose stool in the early morning, poor digestion, persistent diarrhea leading to emaciation, loss of appetite, cold limbs and fatigue. Evaluations were based on general behavioral indicators (huddling, arching back, and lethargy), as well as measurements of anal temperature, food and water intake, fecal water content and body weight.

2.2.3. Measurement of the weight change rate

The mice were weighed on the 1st, 4th, 7th, 11th and 14th days. It's calculated by:

First-week weight change rate (%) = (weight measured - weight for the first day)/weight for the first day × 100 %

Second-week weight change rate (%) = (Weight measured - Weight on day 7)/Weight on day 7 × 100 %

2.2.4. Determination of fecal water content

To determine the fecal water content, mouse feces were collected from days 7–14 of molding, weighed, dried, and then reweighed. Fecal water content (%) is calculated as (wet weight - dry weight)/wet weight times 100 %.

2.2.5. Determination of organ index

The organ indices were calculated based on the whole spleen and thymus weights relative to the body weight. Organ index (%) is calculated as (organ weight/body weight) times 100 %

2.2.6. Determination of the microbiological activity of the small intestinal contents

The specimens were gathered and diluted with sterile water at a ratio of 3 g:50 mL. The mixture was shaken for 90 min on a shaker to disperse the microbial aggregates. The supernatant was collected after centrifugation. Fluorescein diacetate hydrolysis spectrophotometric analysis at 490 nm was used to measure the microbial activity [29].

2.2.7. Determination of TMAO, NLRP3, IL-1β and TGF-β1 contents

After thawing at room temperature, the serum, small intestine and kidney tissues were processed for ELISA analysis. The kidney and small intestine tissues were homogenized, mixed with physiological saline, and centrifuged to collect the supernatant. Standard blanks and sample wells were prepared following the kit instructions. Samples were added, followed by adding enzyme, incubating, washing the plate and adding color. Each sample's concentration was determined using a microplate reader at 450 nm.

2.2.8. Histopathological observation of kidneys

Renal tissues with connective tissue removed were preserved in a 4 % paraformaldehyde solution. The steps were as follows: dewaxing the paraffin sections in water; staining with Masson's staining solution (A, B, C, D, E, F); differentiation with 1 % acetic acid; dehydration; and sealing. Wuhan Xavier Biotechnology Co. (Wuhan, China) was also involved in the experiments above. ImageJ software was used for semiquantitative analysis of the collagen fiber content in renal tissues.

2.2.9. Occludin and ZO-1 expression in small intestinal tissues

Small intestinal tissues (1–2 cm long) with connective tissue removed were fixed in a 4 % glutaraldehyde solution. The steps included dewaxing the paraffin sections, blocking endogenous peroxidase, blocking the serum, incubating the sections with antibodies, staining with DAB, counterstaining the nuclei, dehydrating the sections and sealing the sections. Wuhan Xavier Biotechnology Co. was entrusted with conducting the experiments above. The degree of positive staining was assessed by measuring the average optical density (AOD) of the small intestinal pathological sections using ImageJ software.

2.2.10. 16S rRNA high-throughput sequencing of small intestinal mucosa microbirta

The small intestinal mucosa was used to extract total DNA, and conserved areas were the focus of primer design. The primers that were selected were the upstream (338F: 5′-ACTCCTACGGGGAGGCAGCA-3′) and downstream (806R: 5′-GGACTACHVGGGGTWTC-TAAT-3′). The 16S rRNA V3+V4 region was chosen for PCR amplification. 1.8 % agarose gel electrophoresis was used to analyze the amplified PCR products. NanoDrop 2000 was used to measure the purity of the DNA. The products were then purified, quantified and homogenized to create sequencing libraries. After quality control (QC), the libraries that passed QC were sequenced using an Illumina NovaSeq 6000.

2.2.11. Bioinformatics and statistical analysis

The Amplicon Sequence Variants (ASVs) were denoised, a Venn plot of the ASVs was obtained, and the α and β diversities were assessed using the dada2 method in QIIME2 2020.6 software. Naive Bayes classifiers with the Silva 138 reference database were used to classify and annotate the feature sequences. LEfse analysis detected features with significantly different abundances, and nonparametric tests were used to determine taxonomic units with significantly different abundances. For every group, the effect magnitude of the variations in abundance was estimated using a linear discriminant analysis. With PICRUSt2 software and the Integrated Microbial Genomes database, the functional gene composition was inferred using KEGG pathway information.

The data are shown as mean ± standard deviation and were statistically analyzed using SPSS 25.00 software. For intergroup comparative analysis, independent sample t-tests were employed where the data met the requirements of homoscedasticity and normality. Otherwise, Mann-Whitney *U* test was applied. $\alpha = 0.05$ was used as the significance threshold.

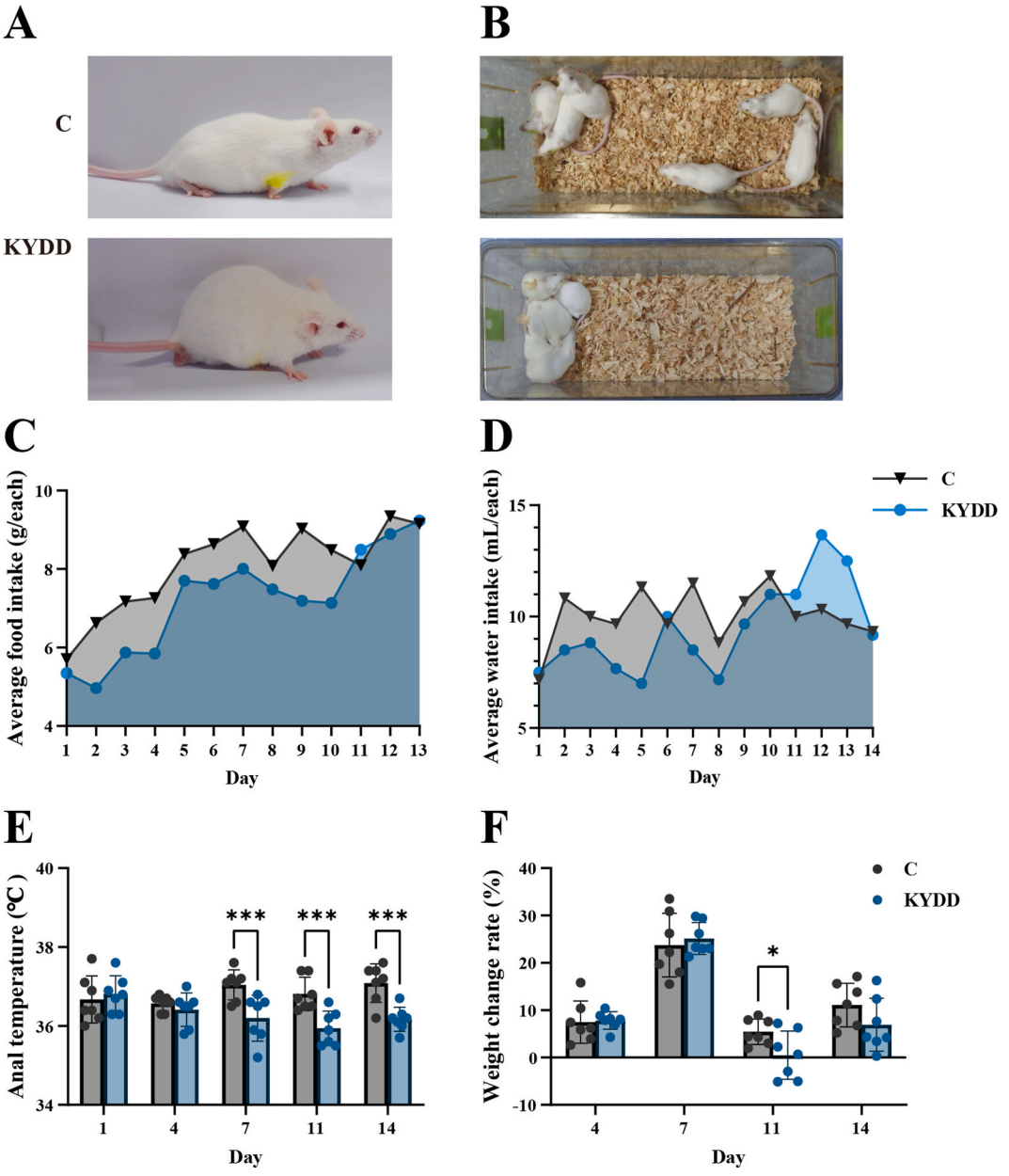

Fig. 1. General behavioral observations and symptoms of the mice. Note: (A) Activity status, (B) Mental status, (C) Average food intake, (D) Average water intake, (E) Anal temperature, (F) Weight changes. The values were expressed as mean ± standard deviation (n = 7 for each group). $^{*}P < 0.05$, $^{***}P < 0.001$.

3. Results

3.1. General behavioral observations and symptoms

The C group was in good condition, had sleek fur, and behaved energetically during the modeling phase. In contrast, the KYDD group exhibited huddling behavior, arched backs, aversion to cold, signs of fatigue, lethargy and dull fur (Fig. 1A and B). The KYDD group exhibited lower food and water intake (Fig. 1C and D), along with a decreasing trend in anal temperature and weight. After administering *Folium Sennae* decoction, the anal temperature of the mice in the KYDD group was significantly lower than the C group ($P < 0.001$; Fig. 1-E). Additionally, on the eleventh day, there was a noticeable decrease in weight ($P < 0.05$) (Fig. 1-F).

3.2. Fecal characteristics and changes in organ indices

The C group mice had clean perianal regions, dry bedding and black pellet-like feces with a moderate consistency that maintained shape when pressed on filter paper. In contrast, the mice in the KYDD group had contaminated perianal regions, moist bedding and soft yellow feces that deformed easily stuck to forceps when picked up and left noticeable watermarks when pressed on filter paper. Additionally, the KYDD group exhibited higher fecal water content (Fig. 2A–D).

The modeling may have triggered an immunological response in the KYDD group as evidenced by the higher spleen and thymus indices observed compared to the C group, with a significant difference in the spleen indices ($P < 0.05$; Fig. 2E and F).

3.3. Changes in microbial activity, TMAO, NLRP3 and IL-1β

The modeling may have impacted microbiota metabolism and inhibited the growth of relevant microbes, as evidenced by the significantly decreased microbial activity in the KYDD group compared to the C group ($P < 0.05$; Fig. 3-A).

Increased TMAO levels were positively correlated with kidney-yang deficiency syndrome diarrhea, as evidenced by the significantly higher TMAO concentrations in the serum, kidney and small intestine of the KYDD group compared to the C group ($P < 0.001$; Fig. 3B–D).

There is a positive association between the inflammatory response and kidney-yang deficiency syndrome diarrhea, as seen by the NLRP3 and IL-1β blood levels in the KYDD group being noticeably greater compared to the C group ($P < 0.001$; Fig. 3E and F).

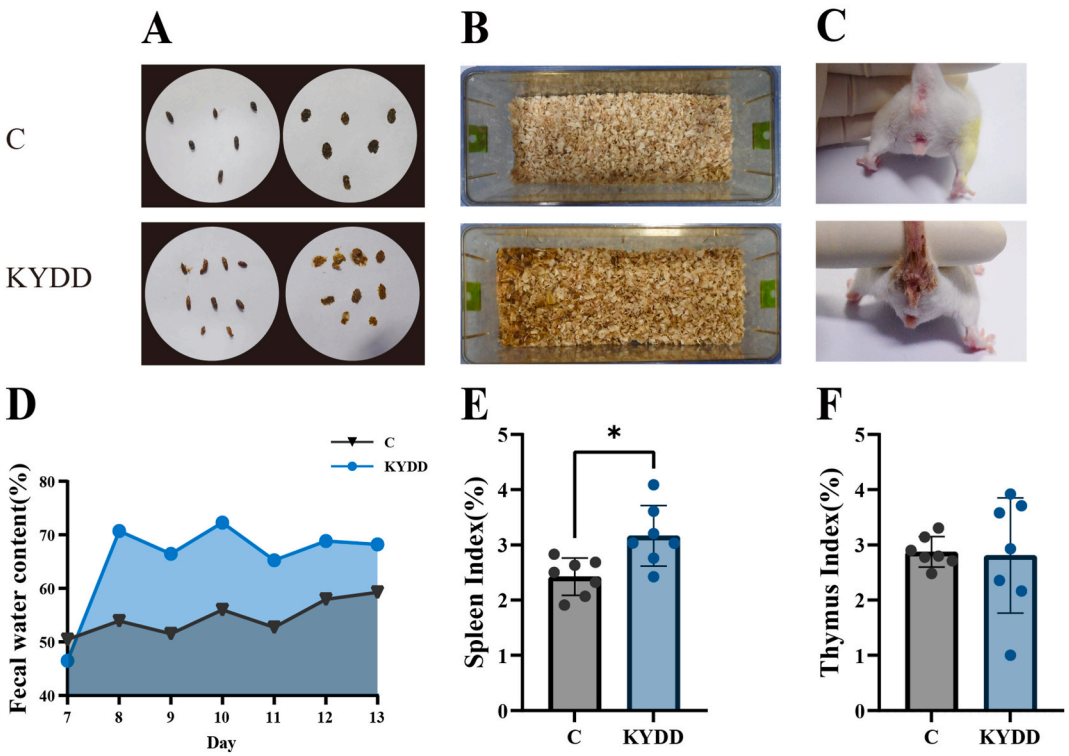

Fig. 2. Effect of modeling on fecal characteristics and organ indices. Note: (A) Fecal characteristics, (B) Cage box humidity, (C) Perianal cleanliness, (D) Fecal water content, (E) Spleen index, (F) Thymus index. The values were expressed as mean ± standard deviation (n = 7 for each group). *$P < 0.05$.

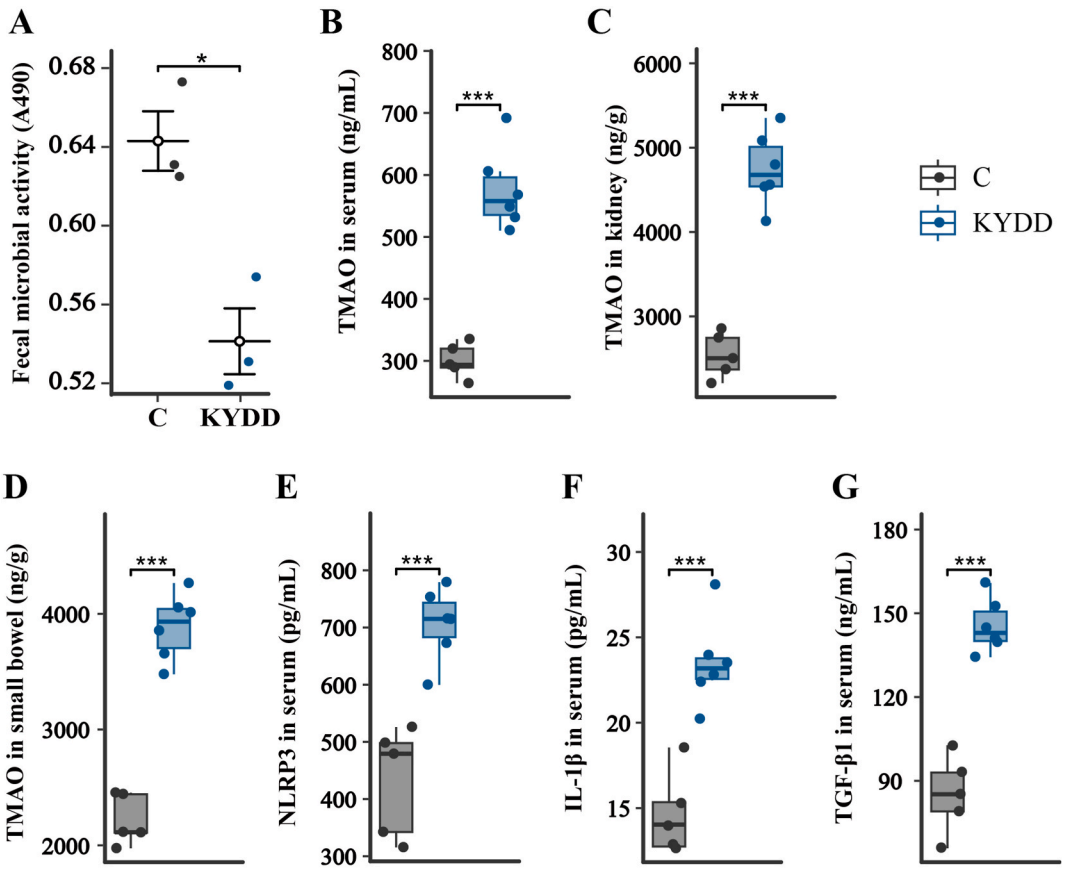

Fig. 3. (A) Changes in microbial activity, (B)Trimethylamine-N-oxide levels in serum, (C) Trimethylamine-N-oxide levels in kidney tissue, (D) Trimethylamine-N-oxide levels in small intestine tissue, (E) NOD-like receptor thermal protein domain associated protein 3 levels in serum, (F) Interleukin-1β levels in serum, (G) Transforming growth factor-β1 levels in serum. The values were expressed as mean ± standard deviation (Figure A: n = 3 for each group; Figure B–G: n = 6 for each group). *$P < 0.05$, ***$P < 0.001$.

3.4. Renal fibrosis and disruption of the intestinal barrier

TGF-β1 is the main factor that promotes renal interstitial fibrosis by regulating the growth, synthesis and secretion of fibroblasts and the extracellular matrix (ECM). Fig. 3-G shows a significant increase in the serum TGF-β1 concentration after modeling ($P < 0.001$). Additionally, as shown in Fig. 4A and B, Masson staining of kidney tissues revealed substantial deposition of blue collagen fibers in the kidney interstitium ($P < 0.001$). These findings suggest that modeling induces some degree of renal fibrosis.

The Occludin and ZO-1 proteins regulate intestinal permeability and maintain tight junction stability, which is essential for ensuring a healthy intestinal barrier in small intestine tissues. Occludin and ZO-1 proteins appeared as brownish-yellow staining in the cytoplasm. The occludin and ZO-1 AODs decreased in the KYDD group, with ZO-1 showing a substantial decline ($P < 0.01$; Fig. 4C–F). As revealed by ZO-1 immunohistochemical staining, the KYDD group showed an increase in small cell clusters with basophilic nuclei. These findings indicate that the modeling process disrupted intestinal barrier integrity.

3.5. Changes in the small intestinal Intestinal microbiota

3.5.1. α and β diversities of intestinal microbiota

α-Diversity measures species richness and diversity and was assessed using the Chao1, Simpson, Shannon and Angiotensin-converting enzyme index (ACE) indices. Higher ACE and Chao1 indices were observed in the KYDD group, suggesting increased species richness in the intestinal microbiota and indicating greater diversity of species (Fig. 5A and B). The intestinal microbiota in the KYDD group also exhibited a higher Shannon index, suggesting a more uniform and varied distribution (Fig. 5-C). Throughout the modeling process, there was a general trend towards increased diversity and species richness in the intestinal microbiota, as indicated by rising diversity indices in the KYDD group. However, these differences did not reach statistical significance.

Microbial communities can be compared and contrasted using β-Diversity analysis through non-metric multidimensional scaling analysis (NMDS) and principal coordinates analysis (PCoA). The findings revealed that although the KYDD group had more internal diversity and notable distinctions, the C group had substantial similarities (Fig. 5E and F). The NMDS analysis yielded a stress value of

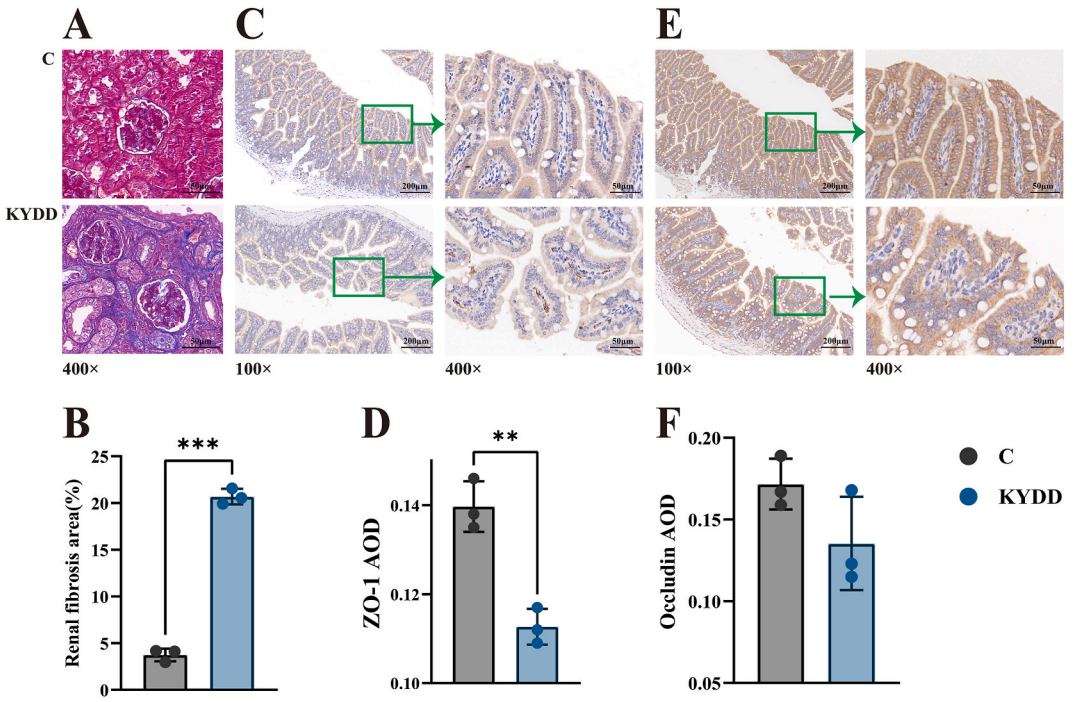

Fig. 4. Effect of modeling on the intestinal barrier. Note: (A) Effect of the model on renal fibrosis (Masson staining, × 400), (B) area of renal fibrosis (Masson semiquantitative), (C) Zonula Occludens-1 protein expression in intestinal tissue (immunohistochemistry × 100, × 400), (D) Zonula Occludens-1 average optical density, (E) Occludin protein expression in intestinal tissue (immunohistochemistry × 100, × 400), (F) Occludin average optical density. The values were expressed as mean ± standard deviation (n = 3 for each group). $^{**}P < 0.01$.

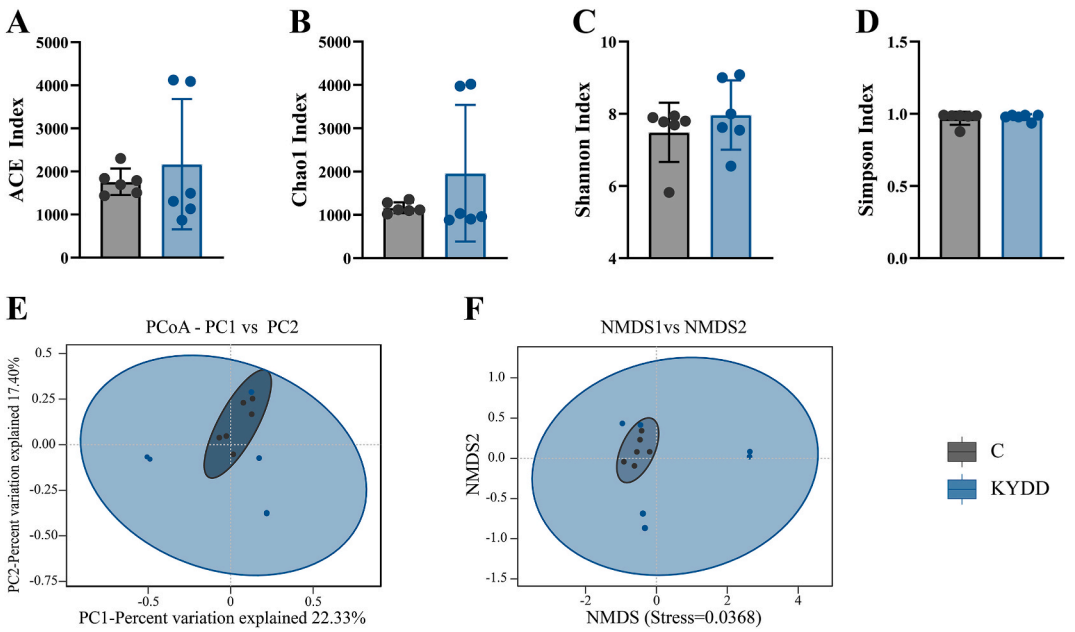

Fig. 5. Diversity analysis of the intestinal intestinal microbiota. Note: (A) Angiotensin-converting enzyme index, (B) Chao1 index, (C) Shannon index, (D) Simpson index, (E) Principal coordinates analysis, (F) Non-metric multidimensional scaling analysis. The values were expressed as mean ± standard deviation (n = 6 for each group).

0.0368 (<0.05), indicating its representativeness and reliability in reflecting changes in the mucosal microbiota due to modeling.

3.5.2. ASV and taxonomic levels analysis of the intestinal Intestinal microbiota

ASVs enable accurate differentiation between sequences at the single nucleotide level. As shown in Fig. 6-A, the C group had 3126 ASVs, the KYDD group had 6109 ASVs, and 573 ASVs were shared between the two groups. These findings indicate that the model altered the microbial community composition of the intestinal mucosal microbiota.

The KYDD group exhibited higher bacterial counts in all taxonomic categories, according to the comparison of changes in taxonomic levels after modeling (Fig. 6-B).

3.5.3. Analysis of dominant intestinal microbiota

Firmicutes, Proteobacteria, Actinobacteria, Bacteroidetes, and Acidobacteria were the primary phyla, according to a comparison of the abundances of the top ten bacterial phyla and genera. Group KYDD exhibited an 11.77 %, 0.90 %, and 1.03 % increase in the relative abundances of Firmicutes, Proteobacteria, and Bacteroidetes as compared to group C. In comparison, the abundances of Actinobacteria and Acidobacteriota decreased by 7.99 % and 0.84 %, respectively, resulting in a 90.10 % increase in the F/B ratio (Fig. 6-C). The findings of the statistical analysis showed that the abundance of Firmicutes had significantly increased ($P < 0.01$), suggesting that the dominating bacterial makeup at the phylum level has changed (Fig. 6-D).

Unclassified Bacteria, *Candidatus Arthromitus*, *Enterococcus*, *unclassified Archaea* and *Corynebacterium* were the dominant bacterial genera at the genus level. Compared to those in group C, the relative abundances of *unclassified Bacteria*, *Enterococcus* and *Corynebacterium* in group KYDD decreased by 6.60 %, 0.99 % and 2.09 %, respectively, while *Candidatus Arthromitus* and *unclassified Archaea* increased by 6.26 % and 1.17 %, respectively (Fig. 6-E). The genus-level dominating bacterial composition appears to be changing, but this trend is not statistically significant (Fig. 6-F).

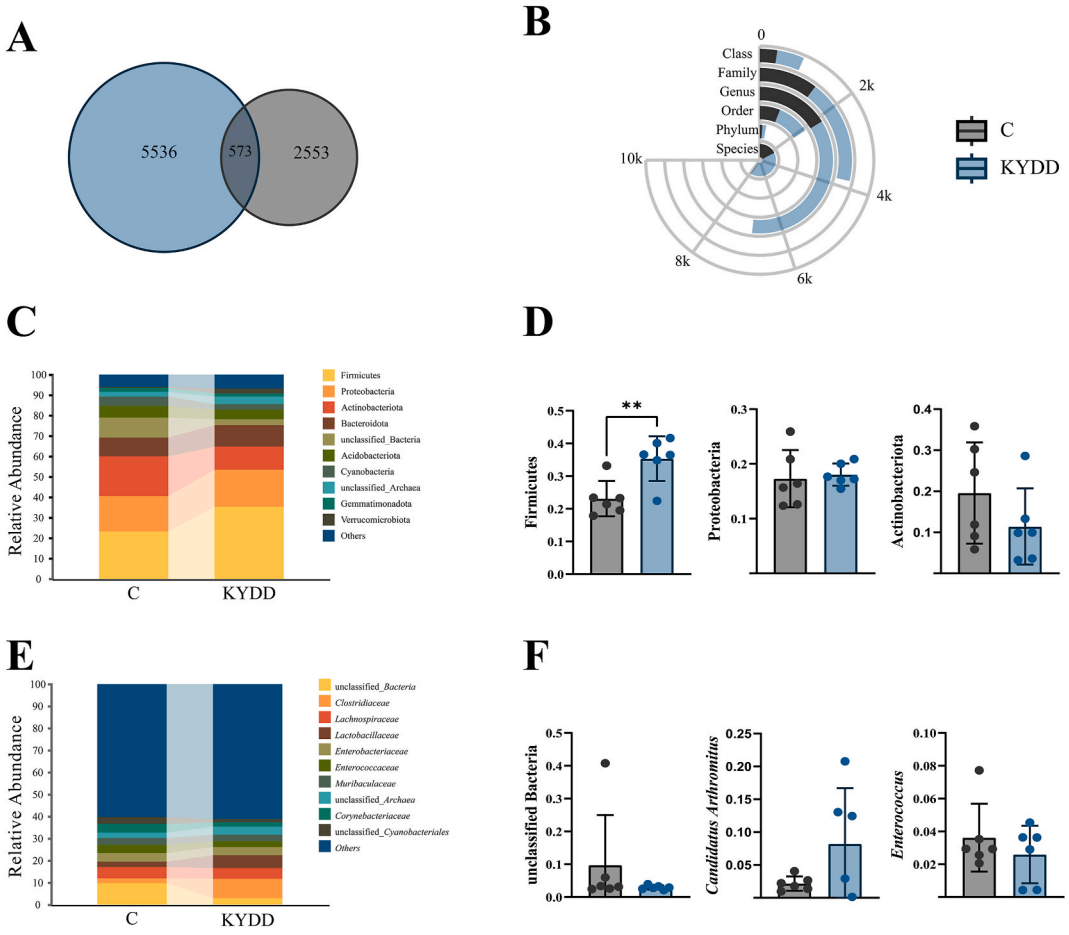

Fig. 6. Structural changes in the intestinal intestinal microbiota. Note: (A) Venn plot of Amplicon Sequence Variants. (B) Interaction yuk jak plot, (C) Phylum-level relative abundance plot, (D) Phylum-level dominant intestinal microbiota, (E) Genus-level relative abundance plot, (F) Genus-level dominant intestinal microbiota. The values were expressed as mean ± standard deviation (n = 6 for each group). $^{**}P < 0.01$.

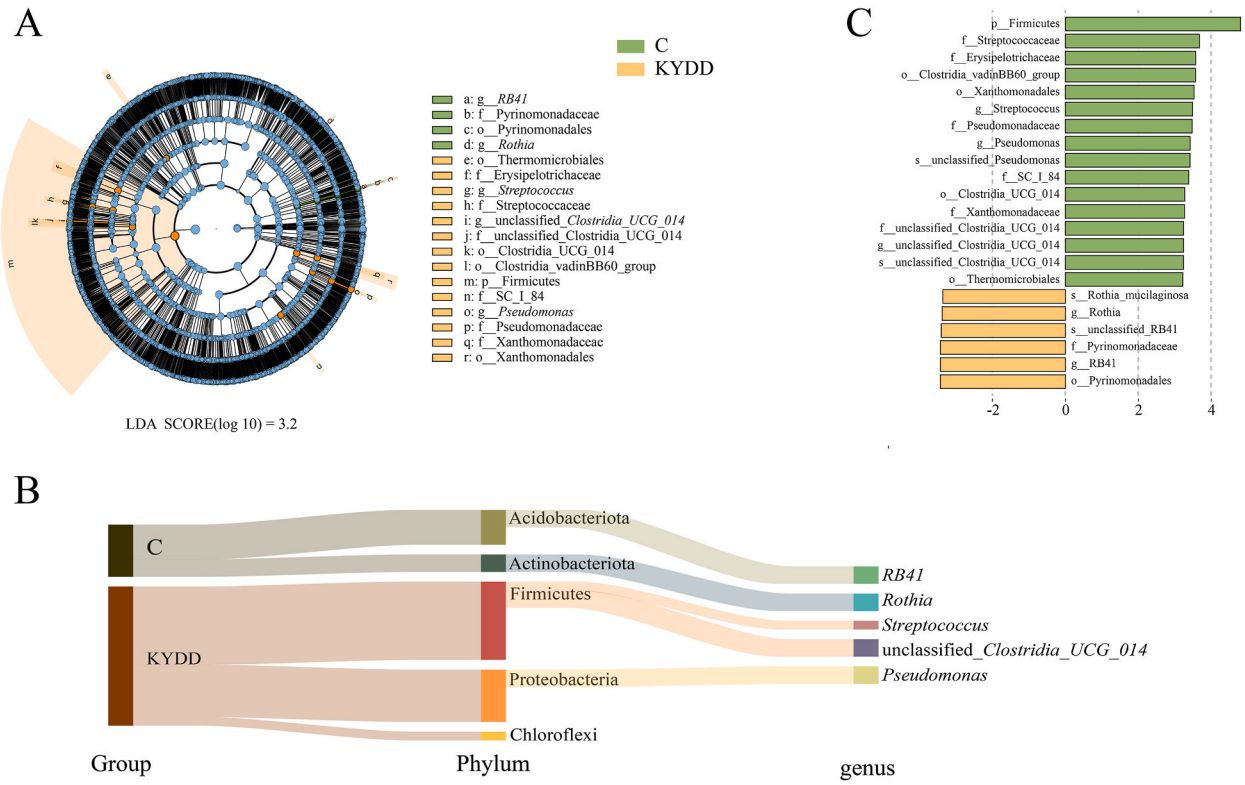

Fig. 7. Characteristics of the intestinal microbiota. Note: (A) Evolutionary branching diagrams, (B) distribution bar charts, (C) subordination tracing Sankey diagrams (n = 6 for each group).

3.5.4. Analysis of the characteristic intestinal microbiota

We utilized LEfSe (LDA score >3.2) to pinpoint significant microbial taxa, aiming to explore variations in the intestinal microbiota between C and KYDD groups (Fig. 7A and B). As depicted in the taxonomic hierarchy in Fig. 7-C, we identified 22 significant differences in the microbial taxa. In the C group, Actinobacteria (including *RB41*) and Acidobacteriota (including *Rothia* and *unclassified Clostridia* UCG 014) were the predominant bacteria, while Firmicutes (including *Streptococcus*), Proteobacteria (including *Pseudomonas*) and Chloroflexi were the dominant bacteria in the KYDD group.

3.5.5. Functional analysis of the intestinal microbiota

Six main functional categories can be used to categorize the intestinal microbiota, with 182 subcategories having a median count >529,138. Among them, 112 categories related to metabolic functions had the highest abundance. Among the top 18 KEGG pathways analyzed, metabolic functions accounted for 76 % of the genes (Fig. 8-A), having a major influence on nucleotide metabolism, energy metabolism, amino acid metabolism, global and summary maps, and carbohydrate metabolism (Fig. 8-B). Though there was no discernible change, the metabolic function of the KYDD group declined in comparison to the C group (Fig. 8-C).

3.5.6. Correlation analysis of the intestinal Microbiota's features with TMAO, inflammatory and renal fibrosis indicator levels

Based on the RDA results shown in Fig. 9-A, *Rothia* and *RB41* were negatively correlated, while *Pseudomonas*, *Streptococcus* and *unclassified Clostridia* UCG 014 were positively correlated with TMAO, NLRP3, IL-1β and TGF-β1. These results indicate a direct correlation between elevated TMAO levels and dysbiosis in the intestinal microbiota, implying a possible function in regulating both the inflammatory response and renal fibrosis.

3.5.7. Correlation analysis of TMAO levels with inflammatory response-related indicators and renal fibrosis-related indicators

RDA and correlation analyses showed that there were strong positive relationships between the levels of TGF-β1, IL-1β, NLRP3 and TMAO (Fig. 9B–E). These findings indicate that TMAO concentrations are positively associated with inflammation and renal fibrosis.

4. Discussion

4.1. Correlations between renal fibrosis, inflammatory response and circulating TMAO levels and changes in the intestinal microbiota

During the modeling period, the model group exhibited signs of cold intolerance, seeking shelter, hunching, and arching their

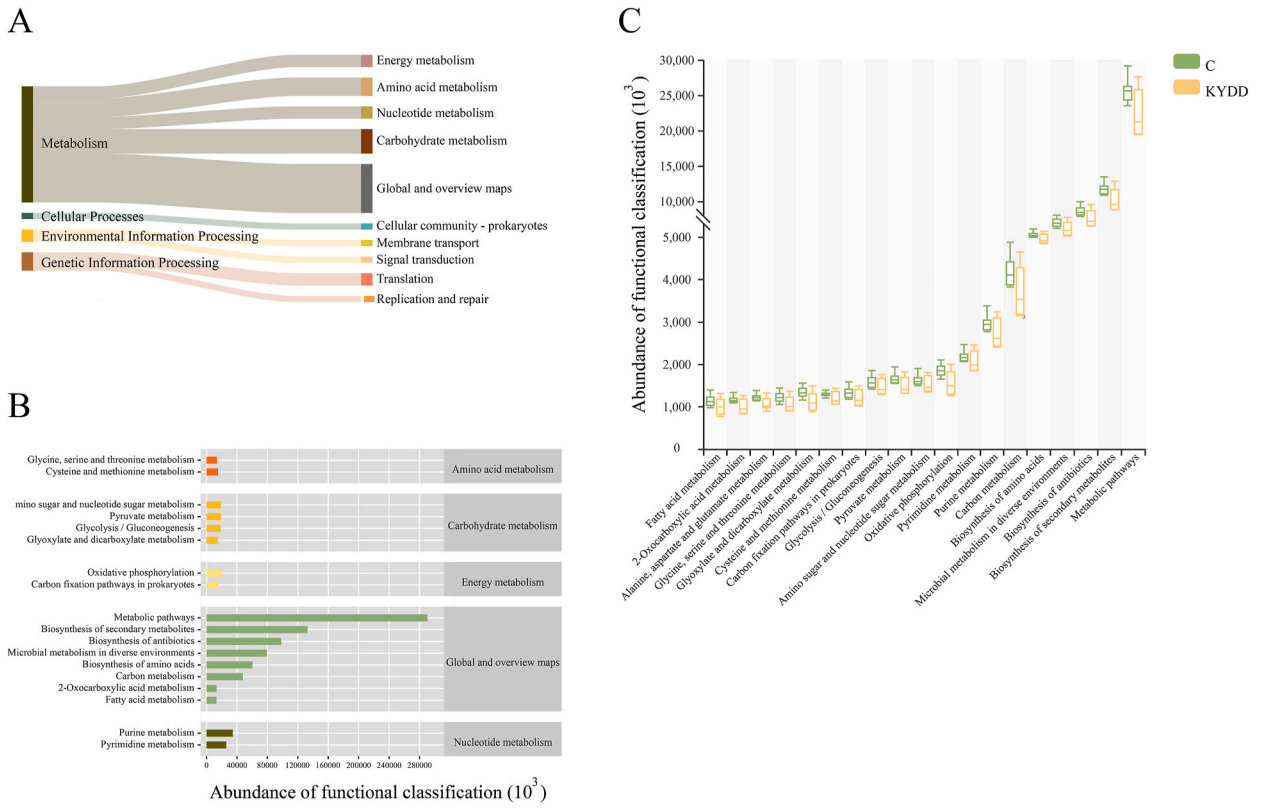

Fig. 8. Functional analysis of the intestinal microbiota. Note: (A) Tracking Sankey plots (Level 1 and Level 2), (B) Functional predictive abundance plots (Level 2 and Level 3), (C) Metabolic function intergroup comparative box line plots (Level 3). The values were expressed as mean ± standard deviation (n = 6 for each group).

backs. Their feces were watery and adhered to forceps, and the bedding was damp. Additionally, they had decreased food and water intake, rectal temperature and body weight, indicating successful model replication.

After modeling, the intestinal microbiota displayed increases in α and β diversities as well as the ASV count. Genes for TMA production, such as carnitine oxygenase (CntA), betain e reductase (GrdH) and cleavage enzyme (CutC), are present in several bacteria. GrdH and CutC-containing bacteria are primarily found in various taxonomic groups within the Firmicutes phylum, whereas CntA is primarily linked to sequences related to *Escherichia* [30,31]. The production of TMA and TMAO by Proteobacteria and Firmicutes is linked to an increased F/B ratio [31–33]. In this study, modeling increased Proteobacteria and Firmicutes relative abundance ($P < 0.05$), which in turn boosted the F/B ratio by 90.10 %. LEfSe and RDA showed that elevated levels of *Streptococcus*, *Pseudomonas*, and *unclassified Clostridia* UCG 014, along with decreased levels of *Rothia* and *RB41*, contributed to the increase in TMAO.

There are 104 known species of gram-positive *streptococcus* bacteria, which are distributed throughout the human body. such as the nasopharynx and gastrointestinal tract. It can interact with host organisms, and some pathogenic species can cause severe invasive infections, resulting in significant illness and death [34,35]. Research has shown that Pseudomonas-mediated quorum sensing (QS) is connected to inflammation and increased intestinal barrier permeability [36]. Pseudomonas causes inflammation and mitochondrial apoptosis in macrophages. It activates the NLRP3 inflammasome through OMV-mediated transfer of toxins, which selectively induces neutrophils to secrete IL-1β [37,38]. Correlation and RDA analysis indicated a positive correlation between *Streptococcus* and *Pseudomonas* with NLRP3, IL-1β and TGF-β1, suggesting that a rise in these bacteria is linked to compromised intestinal barrier function and renal fibrosis.

4.2. TMAO contributes to intestinal barrier disruption and renal fibrosis by transmitting inflammatory cytokines via the "gut-kidney axis"

TMAO induces inflammatory reactions through the activation of inflammasome (primarily NLRP3) and atypical nuclear transcription factor-κB (NF-κB) signaling pathways [39]. Studies have demonstrated that mice administered TMAO injections exhibit increased synthesis of IL-1β and activation of the NLRP3 inflammasome [40]. Carboxyl-terminal leucine-rich repeat (LRR), nucleotide-binding oligomerization domain (NOD) and amino-terminal pyrin domain (PYD) sequences make up the trimeric protein known as NLRP3 [41]. It can activate the downstream inflammatory cell IL-1β [42] and is involved in diarrhea [43]. The current investigation demonstrated a considerable increase in TMAO, NLRP3, and IL-1β levels. RDA and correlation analysis revealed that the TMAO concentration was closely related to the NLRP3 and IL-1β levels, suggesting that TMAO contributes to the inflammation linked

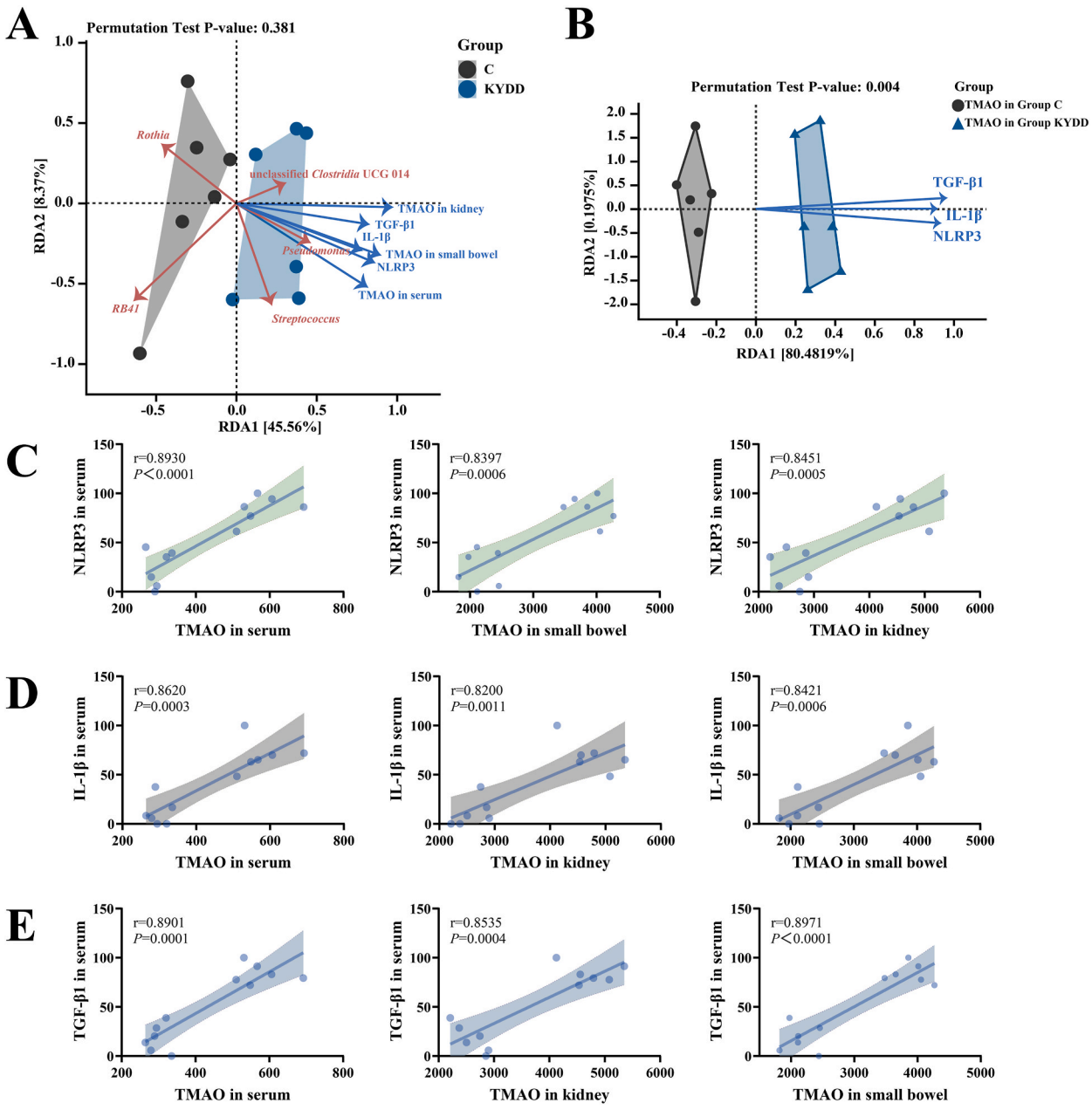

Fig. 9. Correlation analysis. Note: (A) RDA redundancy analysis of mucosal genera associated with trimethylamine-N-oxide, transforming growth factor-β1, interleukin-1β and NOD-like receptor thermal protein domain associated protein 3; (B) RDA redundancy analysis of trimethylamine-N-oxide combined with transforming growth factor-β1, interleukin-1β and NOD-like receptor thermal protein domain associated protein 3; (C) scatter plot of the correlation between trimethylamine-N-oxide and NOD-like receptor thermal protein domain associated protein 3; (D) scatter plot of the correlation between trimethylamine-N-oxide and interleukin-1β; (E) scatter plot of the correlation between trimethylamine-N-oxide and transforming growth factor-β1 (n = 6 for each group).

to kidney-yang deficiency syndrome.

When tissue damage occurs, macrophage play a crucial role in the inflammatory response. Upon activation, macrophages release various cytokines, including IL-1β and TGF-β1 signaling the onset of fibrosis, which frequently occurs with organ inflammatory disorders [44,45]. By promoting the synthesis of extracellular matrix (ECM) and preventing its breakdown, TGF-β1 promotes progressive fibrosis in renal fibrosis [46]. The bidirectional pathogenic effect of TMAO on renal fibrosis has been demonstrated. TMAO is filtered and excreted by the kidney, and its levels increase as renal function declines [8]. Research has demonstrated that TMAO reductase serum levels rise in CKD patients and mice [47]. Additionally, TMAO interacts with TGF-β1/Smad3 pathway. Elevated levels of TMAO promote interstitial fibrosis and collagen deposition in renal tubules, accompanied by increased phosphorylation of Smad3 [48,49].

The kidney's interstitium showed a considerable rise in TGF-β1 and blue collagen fiber deposition in the current investigation. Additionally, TMAO and TGF-β1 showed a favorable association. Through this experiment, we found that TMAO induces inflammatory responses leading to renal fibrosis, which in turn promotes the accumulation of TMAO, resulting in a vicious cycle.

Epithelial barrier disruption and intestinal inflammation may occur concurrently with the onset of CKD, which accelerates bacterial translocation, increases TMAO concentration and leads to renal injury [50]. Basophils are typically present only in the circulation but are rapidly recruited to inflamed tissues [51,52]. Releasing proinflammatory cytokines, including NLRP3 and IL-1β, can increase tight junction permeability and subsequent intestinal barrier dysfunction [53,54]. In adenine-treated rats, the expression of inflammation-related factors significantly increases, accompanied by a considerable drop in the blood levels of ZO-1 and occludin [55]. The tight junction system is mostly dependent on occludin and ZO-1, two typical proteins that control intestinal wall permeability and are essential for preserving the integrity of the intestinal barrier [56,57]. This investigation revealed that there was a considerable increase in the amount of tiny cell clusters with basophilic nuclei in the small bowel villi, concomitant with decreased ZO-1 and occludin expression. These results suggest that TMAO can cause the gut to become inflamed, disrupt the function of the intestinal barrier, increase permeability, and cause bacteria to translocate. Simultaneously, the disrupted intestinal barrier allows additional TMA to enter the bloodstream, thereby increasing the level of TMAO and creating a vicious cycle.

In summary, a rise in TMAO sets off a vicious loop that disrupts the "gut-kidney axis" and eventually serves as a catalyst for kidney-yang deficiency syndrome diarrhea.

5. Conclusion

An unbalanced intestinal bacteria may be associated with elevated levels of TMAO. TMAO triggers inflammation and the transmission of proinflammatory cytokines through the "gut-kidney axis", which contributes to kidney-yang deficiency syndrome diarrhea, leading to intestinal barrier impairment and renal fibrosis. Dysfunction of the "gut-kidney axis" promotes an increase in TMAO levels, thereby forming a vicious cycle.

Ethics approval and consent to participate

The animal tests were authorized by the Hunan University of Traditional Chinese Medicine Animal Ethics and Welfare Committee and met all animal ethics regulations (Ethics No. LLBH-202303190001).

Funding statement

Funding for this research was provided by the Changsha Science and Technology Bureau (kq2208182) and the Hunan Provincial Education Department's Key Scientific Research Project [22A0270].

Availability of data and materials

Online repositories contain the datasets that were used in this investigation. The accession numbers and names are: PRJNA1032712 at https://www.ncbi.nlm.nih.gov/.

CRediT authorship contribution statement

Shiqin Xie: Writing – original draft. **Na Deng:** Writing – original draft. **Leyao Fang:** Writing – original draft. **Junxi Shen:** Writing – original draft. **Zhoujin Tan:** Writing – review & editing. **Ying Cai:** Writing – review & editing.

Declaration of competing interest

The authors declare that they have no competing interests. All the authors have approved the manuscript and agree with this submission.

References

[1] M. Lombardo, G. Aulisa, D. Marcon, G. Rizzo, M.G. Tarsisano, L. Di Renzo, M. Federici, M. Caprio, A. De Lorenzo, Association of urinary and plasma levels of trimethylamine N-oxide (TMAO) with foods, Nutrients 13 (2021), https://doi.org/10.3390/nu13051426.
[2] Z. Wang, E. Klipfell, B.J. Bennett, R. Koeth, B.S. Levison, B. Dugar, A.E. Feldstein, E.B. Britt, X. Fu, Y.M. Chung, et al., Gut flora metabolism of phosphatidylcholine promotes cardiovascular disease, Nature 472 (2011) 57–63, https://doi.org/10.1038/nature09922.
[3] Y. Chen, Z. Weng, Q. Liu, W. Shao, W. Guo, C. Chen, L. Jiao, Q. Wang, Q. Lu, H. Sun, et al., FMO3 and its metabolite TMAO contribute to the formation of gallstones, Biochim. Biophys. Acta, Mol. Basis Dis. 1865 (2019) 2576–2585, https://doi.org/10.1016/j.bbadis.2019.06.016.
[4] M.H. Janeiro, M.J. Ramírez, F.I. Milagro, J.A. Martínez, M. Solas, Implication of trimethylamine N-oxide (TMAO) in disease: potential biomarker or new therapeutic target, Nutrients 10 (2018), https://doi.org/10.3390/nu10101398.
[5] S.I. Sitkin, E.I. Tkachenko, T.Y. Vakhitov, Metabolic dysbiosis of the gut microbiota and its biomarkers, Eksp Klin Gastroenterol 12 (2016) 6–29.
[6] Y. Zhang, Y. Wang, B. Ke, J. Du, TMAO: how intestinal microbiota contributes to heart failure, Transl. Res. 228 (2021) 109–125, https://doi.org/10.1016/j.trsl.2020.08.007.
[7] Z. Wang, Y. Zhao, Intestinal microbiota derived metabolites in cardiovascular health and disease, Protein Cell 9 (2018) 416–431, https://doi.org/10.1007/s13238-018-0549-0.

[8] W.H. Tang, Z. Wang, D.J. Kennedy, Y. Wu, J.A. Buffa, B. Agatisa-Boyle, X.S. Li, B.S. Levison, S.L. Hazen, Intestinal microbiota-dependent trimethylamine N-oxide (TMAO) pathway contributes to both development of renal insufficiency and mortality risk in chronic kidney disease, Circ. Res. 116 (2015) 448–455, https://doi.org/10.1161/circresaha.116.305360.

[9] G.G. Schiattarella, A. Sannino, E. Toscano, G. Giugliano, G. Gargiulo, A. Franzone, B. Trimarco, G. Esposito, C. Perrino, Gut microbe-generated metabolite trimethylamine-N-oxide as cardiovascular risk biomarker: a systematic review and dose-response meta-analysis, Eur. Heart J. 38 (2017) 2948–2956, https://doi.org/10.1093/eurheartj/ehx342.

[10] X. Li, C. Su, Z. Jiang, Y. Yang, Y. Zhang, M. Yang, X. Zhang, Y. Du, J. Zhang, L. Wang, et al., Berberine attenuates choline-induced atherosclerosis by inhibiting trimethylamine and trimethylamine-N-oxide production via manipulating the gut microbiome, NPJ Biofilms Microbiomes 7 (2021) 36, https://doi.org/10.1038/s41522-021-00205-8.

[11] M.L. Chen, L. Yi, Y. Zhang, X. Zhou, L. Ran, J. Yang, J.D. Zhu, Q.Y. Zhang, M.T. Mi, Resveratrol attenuates trimethylamine-N-oxide (TMAO)-Induced atherosclerosis by regulating TMAO synthesis and bile acid metabolism via remodeling of the intestinal microbiota, mBio 7 (2016) e02210, https://doi.org/10.1128/mBio.02210-15, 02215.

[12] P. Evenepoel, R. Poesen, B. Meijers, The gut-kidney axis, Pediatr. Nephrol. 32 (2017) 2005–2014, https://doi.org/10.1007/s00467-016-3527-x.

[13] Y.Y. Chen, D.Q. Chen, L. Chen, J.R. Liu, N.D. Vaziri, Y. Guo, Y.Y. Zhao, Microbiome-metabolome reveals the contribution of gut-kidney axis on kidney disease, J. Transl. Med. 17 (2019) 5, https://doi.org/10.1186/s12967-018-1756-4.

[14] L. Dai, Z.A. Massy, P. Stenvinkel, N.C. Chesnaye, I.A. Larabi, J.C. Alvarez, F.J. Caskey, C. Torino, G. Porto, M. Szymczak, et al., The association between TMAO, CMPF, and clinical outcomes in advanced chronic kidney disease: results from the European QUALity (EQUAL) Study, Am. J. Clin. Nutr. 116 (2022) 1842–1851, https://doi.org/10.1093/ajcn/nqac278.

[15] A.R. Fatkhullina, I.O. Peshkova, A. Dzutsev, T. Aghayev, J.A. McCulloch, V. Thovarai, J.H. Badger, R. Vats, P. Sundd, H.Y. Tang, et al., An interleukin-23-interleukin-22 Axis regulates intestinal microbial homeostasis to protect from diet-induced atherosclerosis, Immunity 49 (2018) 943–957.e949, https://doi.org/10.1016/j.immuni.2018.09.011.

[16] F. Saaoud, L. Liu, K. Xu, R. Cueto, Y. Shao, Y. Lu, Y. Sun, N.W. Snyder, S. Wu, L. Yang, et al., Aorta- and liver-generated TMAO enhances trained immunity for increased inflammation via ER stress/mitochondrial ROS/glycolysis pathways, JCI Insight 8 (2023), https://doi.org/10.1172/jci.insight.158183.

[17] X. Li, X. Peng, B. Qiao, M. Peng, N. Deng, R. Yu, Z. Tan, Gut-kidney impairment process of adenine combined with Folium sennae-induced diarrhea: association with interactions between lactobacillus intestinalis, Bacteroides acidifaciens and acetic acid, inflammation, and kidney function, Cells 11 (2022), https://doi.org/10.3390/cells11203261.

[18] K. Shi, L. Qu, X. Lin, Y. Xie, J. Tu, X. Liu, Z. Zhou, G. Cao, S. Li, Y. Liu, Deep-fried atractylodis rhizoma protects against spleen deficiency-induced diarrhea through regulating intestinal inflammatory response and intestinal microbiota, Int. J. Mol. Sci. 21 (2019), https://doi.org/10.3390/ijms21010124.

[19] J.A. Murray, A. Rubio-Tapia, Diarrhoea due to small bowel diseases, Best Pract. Res. Clin. Gastroenterol. 26 (2012) 581–600, https://doi.org/10.1016/j.bpg.2012.11.013.

[20] K. Zhou, M. Peng, N. Deng, Z. Tan, N. Xiao, Lactase bacteria in intestinal mucosa are associated with diarrhea caused by high-fat and high-protein diet, BMC Microbiol. 22 (2022) 226, https://doi.org/10.1186/s12866-022-02647-2.

[21] C. Li, N. Xiao, N. Deng, D. Li, Z. Tan, M. Peng, Dose of sucrose affects the efficacy of Qiweibaizhu powder on antibiotic-associated diarrhea: association with intestinal mucosal microbiota, short-chain fatty acids, IL-17, and MUC2, Front. Microbiol. 14 (2023) 1108398, https://doi.org/10.3389/fmicb.2023.1108398.

[22] E.S. John, S. Chokhavatia, Targeting small bowel receptors to treat constipation and diarrhea, Curr. Gastroenterol. Rep. 19 (2017) 31, https://doi.org/10.1007/s11894-017-0573-x.

[23] Y. Li, Z. Yuan, Z. Tan, Correlation between intestinal flora and traditional Chinese medicine syndromes of diarrhea: a review, Chin. J. Exp. Tradit. Med. Formulae (2021) 209–217, https://doi.org/10.13422/j.cnki.syfjx.20211698.

[24] J. Zhu, X. Li, N. Deng, X. Peng, Z. Tan, Diarrhea with deficiency kidney-yang syndrome caused by adenine combined with Folium senna was associated with gut mucosal microbiota, Front. Microbiol. 13 (2022) 1007609, https://doi.org/10.3389/fmicb.2022.1007609.

[25] Y. Wu, X. Peng, X. Li, D. Li, Z. Tan, R. Yu, Sex hormones influence the intestinal microbiota composition in mice, Front. Microbiol. 13 (2022) 964847, https://doi.org/10.3389/fmicb.2022.964847.

[26] M. Zhou, X. Li, J. Liu, Y. Wu, Z. Tan, N. Deng, Adenine's impact on mice's gut and kidney varies with the dosage administered and relates to intestinal microorganisms and enzyme activities, 3 Biotech 14 (2024) 88, https://doi.org/10.1007/s13205-024-03959-y.

[27] X. Li, J. Zhu, Y. Wu, Z. Tan, Correlation between kidney function and intestinal biological characteristics of adenine and Folium SennaeInduced diarrhea model in mice, Turk. J. Gastroenterol. 34 (2023) 4–12, https://doi.org/10.5152/tjg.2022.211010.

[28] S.S. Zhang, C.J. Wang, Y.F. Li, N. Wang, Consensus opinion on TCM diagnosis and treatment of diarrhea, J. Tradit. Chin. Med. 58 (2017) 1256–1260, https://doi.org/10.13288/j.11-2166/r.2017.14.023.

[29] K. Zhou, X. Yi, Z. Tan, M. Peng, N. Xiao, Baohe pill decoction treats diarrhea induced by high-fat and high-protein diet by regulating lactase-producing bacteria in intestinal mucosa, Front. Microbiol. 14 (2023) 1157475, https://doi.org/10.3389/fmicb.2023.1157475.

[30] S. Rath, T. Rud, D.H. Pieper, M. Vital, Potential TMA-producing bacteria are ubiquitously found in mammalia, Front. Microbiol. 10 (2019) 2966, https://doi.org/10.3389/fmicb.2019.02966.

[31] S. Rath, B. Heidrich, D.H. Pieper, M. Vital, Uncovering the trimethylamine-producing bacteria of the human intestinal microbiota, Microbiome 5 (2017) 54, https://doi.org/10.1186/s40168-017-0271-9.

[32] C.E. Cho, S. Taesuwan, O.V. Malysheva, E. Bender, N.F. Tulchinsky, J. Yan, J.L. Sutter, M.A. Caudill, Trimethylamine-N-oxide (TMAO) response to animal source foods varies among healthy young men and is influenced by their intestinal microbiota composition: a randomized controlled trial, Mol. Nutr. Food Res. 61 (2017), https://doi.org/10.1002/mnfr.201600324.

[33] T. Wu, Y. Gao, J. Hao, J. Geng, J. Zhang, J. Yin, R. Liu, W. Sui, L. Gong, M. Zhang, Capsanthin extract prevents obesity, reduces serum TMAO levels and modulates the intestinal microbiota composition in high-fat-diet induced obese C57BL/6J mice, Food Res. Int. 128 (2020) 108774, https://doi.org/10.1016/j.foodres.2019.108774.

[34] C.P. Andam, W.P. Hanage, Mechanisms of genome evolution of Streptococcus, Infect. Genet. Evol. 33 (2015) 334–342, https://doi.org/10.1016/j.meegid.2014.11.007.

[35] J.B. Goldberg, Pseudomonas: global bacteria, Trends Microbiol. 8 (2000) 55–57, https://doi.org/10.1016/s0966-842x(99)01671-6.

[36] P. Deo, S.H. Chow, M.L. Han, M. Speir, C. Huang, R.B. Schittenhelm, S. Dhital, J. Emery, J. Li, B.T. Kile, et al., Mitochondrial dysfunction caused by outer membrane vesicles from Gram-negative bacteria activates intrinsic apoptosis and inflammation, Nat Microbiol 5 (2020) 1418–1427, https://doi.org/10.1038/s41564-020-0773-2.

[37] M.S. Minns, K. Liboro, T.S. Lima, S. Abbondante, B.A. Miller, M.E. Marshall, J. Tran Chau, A. Roistacher, A. Rietsch, G.R. Dubyak, E. Pearlman, NLRP3 selectively drives IL-1β secretion by Pseudomonas aeruginosa infected neutrophils and regulates corneal disease severity, Nat. Commun. 14 (2023) 5832, https://doi.org/10.1038/s41467-023-41391-7.

[38] V.K. Singh, M. Almpani, K.M. Wheeler, L.G. Rahme, Interconnections of Pseudomonas aeruginosa quorum-sensing systems in intestinal permeability and inflammation, mBio 14 (2023) e0352422, https://doi.org/10.1128/mbio.03524-22.

[39] X. Zhang, Y. Li, P. Yang, X. Liu, L. Lu, Y. Chen, X. Zhong, Z. Li, H. Liu, C. Ou, et al., Trimethylamine-N-Oxide promotes vascular calcification through activation of NLRP3 (Nucleotide-Binding domain, leucine-rich-containing family, pyrin domain-containing-3) inflammasome and NF-κB (nuclear factor κB) signals, Arterioscler. Thromb. Vasc. Biol. 40 (2020) 751–765, https://doi.org/10.1161/atvbaha.119.313414.

[40] K.M. Boini, T. Hussain, P.L. Li, S. Koka, Trimethylamine-N-Oxide instigates NLRP3 inflammasome activation and endothelial dysfunction, Cell. Physiol. Biochem. 44 (2017) 152–162, https://doi.org/10.1159/000484623.

[41] B.Z. Shao, Z.Q. Xu, B.Z. Han, D.F. Su, C. Liu, NLRP3 inflammasome and its inhibitors: a review, Front. Pharmacol. 6 (2015) 262, https://doi.org/10.3389/fphar.2015.00262.

[42] S.M. Choudhury, X. Ma, Z. Zeng, Z. Luo, Y. Li, X. Nian, Y. Ma, Z. Shi, R. Song, Z. Zhu, et al., Senecavirus a 3D interacts with NLRP3 to induce IL-1β production by activating NF-κB and ion channel signals, Microbiol. Spectr. 10 (2022) e0209721, https://doi.org/10.1128/spectrum.02097-21.
[43] X. Chen, Q. Kong, X. Zhao, C. Zhao, P. Hao, I. Irshad, H. Lei, M.F. Kulyar, Z.A. Bhutta, H. Ashfaq, et al., Sodium acetate/sodium butyrate alleviates lipopolysaccharide-induced diarrhea in mice via regulating the intestinal microbiota, inflammatory cytokines, antioxidant levels, and NLRP3/Caspase-1 signaling, Front. Microbiol. 13 (2022) 1036042, https://doi.org/10.3389/fmicb.2022.1036042.
[44] W.J. Zhang, S.J. Chen, S.C. Zhou, S.Z. Wu, H. Wang, Inflammasomes and fibrosis, Front. Immunol. 12 (2021) 643149, https://doi.org/10.3389/fimmu.2021.643149.
[45] A. Pellicoro, P. Ramachandran, J.P. Iredale, J.A. Fallowfield, Liver fibrosis and repair: immune regulation of wound healing in a solid organ, Nat. Rev. Immunol. 14 (2014) 181–194, https://doi.org/10.1038/nri3623.
[46] H.Y. Lan, Diverse roles of TGF-β/Smads in renal fibrosis and inflammation, Int. J. Biol. Sci. 7 (2011) 1056–1067, https://doi.org/10.7150/ijbs.7.1056.
[47] S. Boonhai, K. Bootdee, W. Saisorn, K. Takkavatakarn, P. Sitticharoenchai, S. Tungsanga, K. Tiranathanagul, A. Leelahavanichkul, TMAO reductase, a biomarker for gut permeability defect induced inflammation, in mouse model of chronic kidney disease and dextran sulfate solution-induced mucositis, Asian Pac. J. Allergy Immunol. 41 (2023) 168–178, https://doi.org/10.12932/ap-100321-1084.
[48] W. Wu, X. Wang, X. Yu, H.Y. Lan, Smad3 signatures in renal inflammation and fibrosis, Int. J. Biol. Sci. 18 (2022) 2795–2806, https://doi.org/10.7150/ijbs.71595.
[49] Y. Lai, H. Tang, X. Zhang, Z. Zhou, M. Zhou, Z. Hu, F. Zhu, L. Zhang, J. Nie, Trimethylamine-N-Oxide aggravates kidney injury via activation of p38/MAPK signaling and upregulation of HuR, Kidney Blood Press. Res. 47 (2022) 61–71, https://doi.org/10.1159/000519603.
[50] J. Rysz, B. Franczyk, J. Ławiński, R. Olszewski, A. Ciałkowska-Rysz, A. Gluba-Brzózka, The impact of CKD on uremic toxins and intestinal microbiota, Toxins 13 (2021), https://doi.org/10.3390/toxins13040252.
[51] K.D. Stone, C. Prussin, D.D. Metcalfe, IgE, mast cells, basophils, and eosinophils, J. Allergy Clin. Immunol. 125 (2010) S73–S80, https://doi.org/10.1016/j.jaci.2009.11.017.
[52] Y. Yamanishi, H. Karasuyama, Basophils and mast cells in immunity and inflammation, Semin. Immunopathol. 38 (2016) 535–537, https://doi.org/10.1007/s00281-016-0582-0.
[53] L.W. Kaminsky, R. Al-Sadi, T.Y. Ma, IL-1β and the intestinal epithelial tight junction barrier, Front. Immunol. 12 (2021) 767456, https://doi.org/10.3389/fimmu.2021.767456.
[54] Y. Feng, Y. Huang, Y. Wang, P. Wang, H. Song, F. Wang, Antibiotics induced intestinal tight junction barrier dysfunction is associated with microbiota dysbiosis, activated NLRP3 inflammasome and autophagy, PLoS One 14 (2019) e0218384, https://doi.org/10.1371/journal.pone.0218384.
[55] J. Xie, X. Ma, Y. Zheng, N. Mao, S. Ren, J. Fan, Panax notoginseng saponins alleviate damage to the intestinal barrier and regulate levels of intestinal microbes in a rat model of chronic kidney disease, Ren. Fail. 44 (2022) 1948–1960, https://doi.org/10.1080/0886022x.2022.2143378.
[56] A. Fasano, Zonulin and its regulation of intestinal barrier function: the biological door to inflammation, autoimmunity, and cancer, Physiol. Rev. 91 (2011) 151–175, https://doi.org/10.1152/physrev.00003.2008.
[57] C. Schwayer, S. Shamipour, K. Pranjic-Ferscha, A. Schauer, M. Balda, M. Tada, K. Matter, C.P. Heisenberg, Mechanosensation of tight junctions depends on ZO-1 phase separation and flow, Cell 179 (2019) 937–952.e918, https://doi.org/10.1016/j.cell.2019.10.006.